

Dynamics of an Interactive Network Composed of a Bacterial Two-Component System, a Transporter and K^+ as Mediator

Ralf Heermann¹, Katja Zigann¹, Stefan Gayer², Maria Rodriguez-Fernandez³, Julio R. Banga³, Andreas Kremling², Kirsten Jung^{1*}

1 Center for Integrated Protein Science Munich (CiPSM) at the Department Biology I, Microbiology, Ludwig-Maximilians-Universität München, Martinsried, Germany, **2** Fachgebiet für Systembiotechnologie, Technische Universität München, Garching b. München, Germany, **3** BioProcess Engineering Group, IIM-CSIC, Spanish Council for Scientific Research, Vigo, Spain

Abstract

KdpD and KdpE form a histidine kinase/response regulator system that senses K^+ limitation and induces the *kdpFABC* operon, which encodes a high-affinity K^+ uptake complex. To define the primary stimulus perceived by KdpD we focused in this study on the dynamics of the Kdp response. *Escherichia coli* cells were subjected to severe K^+ limitation, and all relevant parameters of the Kdp response, i.e., levels of *kdpFABC* transcripts and KdpFABC proteins, as well as extra- and intracellular K^+ concentrations, were quantitatively analysed over time (0 to 180 min). Unexpectedly, induction of *kdpFABC* was found to follow a non-monotonic time-course. To interpret this unusual behaviour, a mathematical model that adequately captures the dynamics of the Kdp system was established and used for simulations. We found a strong correlation between KdpD/KdpE activation and the intracellular K^+ concentration, which is influenced by the uptake of K^+ via the KdpFABC complex. Based on these results a model is proposed in which KdpD/KdpE phosphorylation is inversely correlated with the intracellular K^+ concentration. To corroborate this hypothesis an isogenic mutant that produces a defective KdpFABC complex, and the *trans*-complemented mutant that expresses the KtrAB high-affinity K^+ uptake system of *Vibrio alginolyticus* were quantitatively analysed. Experimental data and simulations for the mutants consistently support the tight correlation between KdpD/KdpE activation and the intracellular K^+ concentration. This study presents a striking example of the non-intuitive dynamics of a functional unit comprising signalling proteins and a transporter with K^+ as mediator.

Citation: Heermann R, Zigann K, Gayer S, Rodriguez-Fernandez M, Banga JR, et al. (2014) Dynamics of an Interactive Network Composed of a Bacterial Two-Component System, a Transporter and K^+ as Mediator. PLoS ONE 9(2): e89671. doi:10.1371/journal.pone.0089671

Editor: Hendrik W. van Veen, University of Cambridge, United Kingdom

Received: November 19, 2013; **Accepted:** January 21, 2014; **Published:** February 28, 2014

Copyright: © 2014 Heermann et al. This is an open-access article distributed under the terms of the Creative Commons Attribution License, which permits unrestricted use, distribution, and reproduction in any medium, provided the original author and source are credited.

Funding: This work was financially supported by the Deutsche Forschungsgemeinschaft (Exc114/1+2 and JU270/15-1) and the BMBF (SysMO, project 4). MRF and JRB acknowledge financial support from the EU ERASysBio programme and the Spanish MICINN and MINECO (SYSMO grant KOSMOBAC, ref. GEN2006-27747-E/SYS and project MultiScales ref. DPI2011-28112-C04-03; both with partial support from the European Regional Development Fund). The funders had no role in study design, data collection and analysis, decision to publish, or preparation of the manuscript.

Competing Interests: The authors have declared that no competing interests exist.

* E-mail: jung@lmu.de

Introduction

An adequate supply of the monovalent cation K^+ is vital for the survival of all living organisms. It is required for the regulation of cell turgor [1] and pH homeostasis [2], for activation of various enzymes [3] or transporters [4], for gene expression [5–7], translation [8], and the regulation of stress responses [9,10]. *E. coli* possesses three K^+ uptake complexes. Two of these, TrkG/TrkH and Kup, are constitutively produced and have low affinities for K^+ [11,12]. The third one, the high-affinity K^+ transport complex KdpFABC, is only induced when the other transporters are unable to supply the cell's requirement for K^+ [1,13,14]. This situation occurs under conditions of K^+ limitation (at extracellular K^+ concentrations <2 mM), mutation of *trk*, or under hyperosmotic stress imposed by NaCl [15].

Expression of the *kdpFABC* operon is controlled by the histidine kinase/response regulator system KdpD/KdpE [16,17] (Fig. 1). Among two-component systems, the KdpD/KdpE pair is the most widespread. Homologous systems have been found in more than 1000 bacterial and archaeal species, including many

pathogens [18]. Upon activation, the histidine kinase KdpD autophosphorylates and transfers the phosphoryl group to the response regulator KdpE by means of its intrinsic kinase activity [19]. Phosphorylated KdpE exhibits increased affinity for the *kdpFABC* promoter and thereby triggers transcription of the operon (Fig. 1) [20]. The enzymatic activities of purified KdpD and KdpE have been characterized *in vitro* [21]. In particular, KdpD has been shown to be the only protein that dephosphorylates phospho-KdpE and, consequently, it also turns off *kdpFABC* expression (phosphatase activity) (Fig. 1) [21].

The nature of the primary stimulus perceived by KdpD remains contentious. Epstein and coworkers proposed that KdpD senses a decrease in turgor or some effect thereof [15,22]. However, measurements of the volume of cells exposed to different external osmolytes have revealed that reduction of turgor cannot be the primary stimulus for KdpD [23]. Various groups have argued for $[K^+]$ as the control signal for KdpD, and suggested that the primary stimulus might be either the level of intracellular K^+ , processes associated with K^+ transport, or the external K^+ concentration [24–26]. It is important to note that the level of

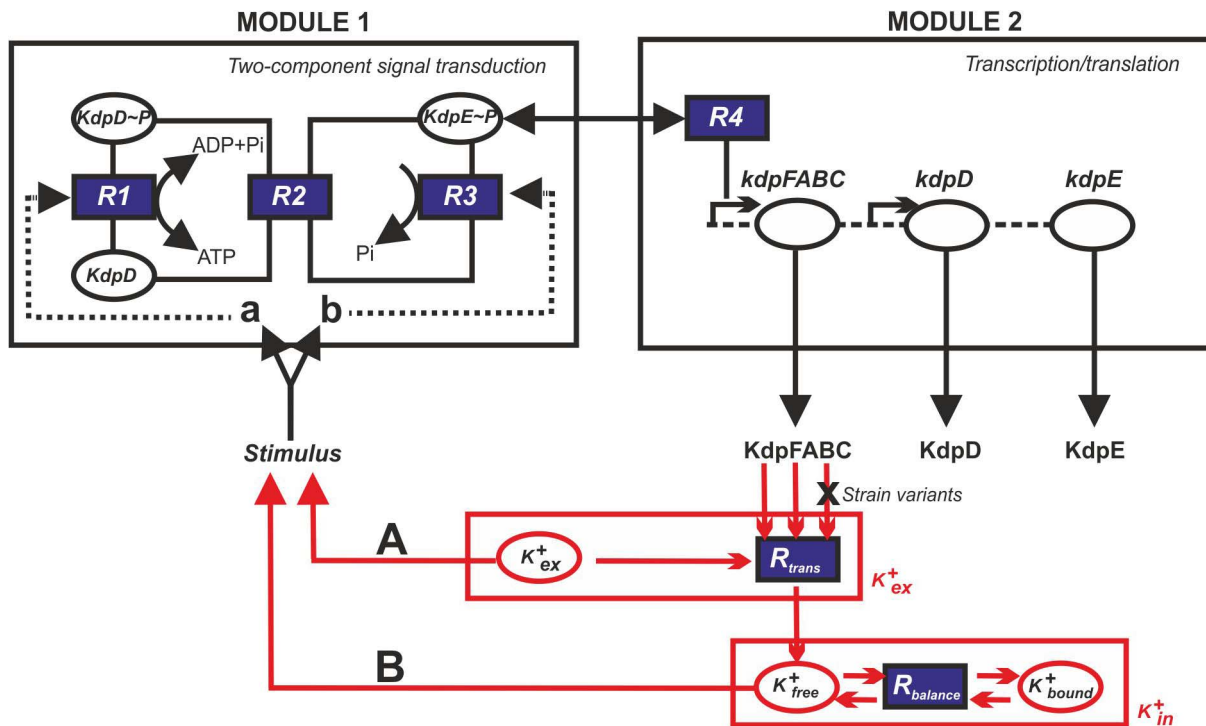


Figure 1. Basic scheme used to construct the mathematical model of the Kdp system. The model is made up of two modules: two-component signal transduction and transcription/translation. The input to the first module is the activating stimulus for KdpD, which results in phosphorylated KdpE, the input to the second module. The output of this module is the production of KdpFABC. The two modules are also linked by a feedback loop from KdpFABC to the KdpD/KdpE system with K⁺ as the mediator. This model reflects the uptake of external K⁺ (K⁺_{ex}) by KdpFABC and the concomitant effects on the balance of intracellular K⁺ in the bound (K⁺_{bound}) and free form (K⁺_{free}). Two potential primary stimuli for KdpD are considered: the external K⁺ concentration (A) and the internal K⁺ concentration (B). Furthermore, K⁺ may affect either the kinase (a) or the phosphatase (b) of KdpD.

doi:10.1371/journal.pone.0089671.g001

kdpFABC expression is at least ten-fold higher under K⁺ limitation than that induced in response to salt stress, which argues for a specific effect of K⁺ on KdpD [23,27]. The observation that extracellular Cs⁺, which is taken up and significantly reduces the availability of free intracellular K⁺, induces *kdpFABC* expression [27] also supports this idea. Furthermore, it has been reported that the fall in internal K⁺ concentrations seen in *E. coli* exposed to acid stress is accompanied by an increase in *kdpFABC* expression [28]. *In vitro* phosphorylation assays based on right-side-out membrane vesicles have revealed an inhibitory effect of K⁺ on the kinase activity of KdpD [29]. An inhibitory effect of K⁺ has also been observed during the *in vitro* reconstitution of the complete signal transduction cascade, consisting of KdpD in proteoliposomes, purified KdpE, a DNA fragment comprising the KdpE-binding site, and a mixture of ATP/ADP. The higher the K⁺ concentration, the lower the level of phosphorylated KdpE [30,31]. These data argue for an effect of the intracellular K⁺ concentration on the activity of KdpD. However, more recent studies have indicated that KdpD activation cannot be solely attributed to the intracellular K⁺ content, and that the extracellular K⁺ concentration also plays a role [32].

To complete this picture it should be noted here that KdpD activity is also modulated by alterations in the ionic strength [29] and by ATP via a regulatory ATP-binding site [33,34]. Furthermore, under conditions of salt stress, UspC provides a scaffold for the KdpD/KdpE signalling cascade and thereby supports phosphorylation in this particular context [30,35].

Thus the data collected over the years have not provided a definitive answer to the question of the nature of the primary stimulus for the KdpD/KdpE system. This is largely because it is difficult to determine the various functional states of KdpD and KdpE *in vivo*. Quantitative analyses of components of biochemical reaction pathways are generally problematic, and represent a real challenge in the life sciences. Mathematical modelling, which allows one to reconstruct biochemical reaction networks *in silico*, provides one way around this impasse. Especially in cases where there is uncertainty about interactions between biochemical compounds, model analysis can help to decide whether certain network topologies can explain experimental observations. Given some prior knowledge or assumptions about the reactions they are involved in, the dynamic behaviour of unmeasured parameters can be simulated. Hence such models can also yield virtual “measurements” of these networks.

To elucidate how K⁺ affects the KdpD/KdpE system *in vivo*, we combined a quantitative experimental analysis with mathematical modelling. First we extended and modified an existing model of the Kdp system (Fig. 1) [36]. Then, we directly monitored and theoretically modelled the time-resolved dynamics of the most salient parameters of the Kdp system in the wild type strain and in selected mutant strains. Our data provide, for the first time, a detailed picture of this highly dynamic interactive network involving two signalling proteins and one K⁺ transporter, in which K⁺ ions serve as major control parameter during adaptation of *E. coli* to persistent stress under K⁺ limitation.

Results

Description of the Kdp system

The Kdp system was previously described by a model consisting of two modules linked by a black box representing a negative feedback loop from KdpFABC to KdpD/KdpE (Fig. 1) [36]. Specifically, the first module describes the autophosphorylation of KdpD, transfer of the phosphoryl group from phospho-KdpD (KdpD-P) to KdpE, dephosphorylation of phospho-KdpE (KdpE-P) yielding inorganic phosphate, and binding of KdpE-P to the *kdp* promoter. The second module accounts for the processes leading to KdpFABC production, and describes the changing numbers of *kdpFABC* transcripts per cell, based on rates of synthesis and degradation of the *kdpFABC* mRNA, and rates of synthesis, turnover and destruction of the proteins KdpFABC, KdpD and KdpE. The feedback loop linking KdpFABC to the first module is now elaborated by a more detailed dynamic model that incorporates the uptake of external K⁺ by KdpFABC and changes in the sizes of free and bound intracellular K⁺ pools (Fig. 1).

Time-resolved dynamics of the Kdp system in *E. coli*

To obtain a time-resolved dataset, samples were collected from an exponential-phase culture of *E. coli* MG1655 growing in a medium containing 10 mM K⁺ and transferred to conditions of severe K⁺ limitation (0.04 mM K⁺) at time zero (Fig. 2). The extracellular K⁺ concentration remained nearly constant for the first 10 min after the shift (Fig. 2A). Then, concomitantly with rising numbers of KdpFABC complexes, K⁺ vanished from the medium at a constant rate, and was completely used up after 45 min (Fig. 2A). This behaviour can be attributed to transport of the ion by the high-affinity K⁺ uptake system KdpFABC, since the constitutively produced Trk (K_m between 1 to 2 mM [11]) is essentially unable to transport K⁺ into the cell under these conditions, while the third K⁺ import system Kup has no impact on rates of K⁺ uptake at neutral pH [37]. These constraints may also account for the initial delay in the onset of uptake after transfer.

The changes in the number of *kdpFABC* transcripts per cell over time were quantified by qRT-PCR (Fig. 2B). Transcription was induced immediately after the shift, and transcript levels increased to reach a maximum after 15 min. Thereafter, transcript levels fell by about 50% to reach a minimum at t = 30 min. At t = 40 min, *kdpFABC* transcript numbers began to rise again, ultimately attaining a maximum that was approximately 40% higher than the first peak. This level was then maintained until the end of the experiment at t = 180 min (Fig. 2B).

In parallel, we used quantitative Western blot analysis to measure the numbers of KdpFABC molecules translated from *kdpFABC* transcripts (Fig. 2C). After a short lag period (the time required for protein synthesis), the number of KdpFABC complexes steadily increased in cells exposed to K⁺ limitation. Within 30 min a level of about 5,000 molecules per cell was reached. Then the net rate of production of KdpFABC complexes decreased, coincidentally with the drop in the numbers of *kdpFABC* transcripts per cell, and was maintained at that level until t = 90 min. The number of KdpFABC complexes showed no further increase thereafter, remaining at a level of about 8,000 per cell. Thus, the net rate of synthesis of KdpFABC complexes followed a hyperbolic time-course.

To complete the dataset, we also measured the changes in intracellular K⁺ concentration. It is important to note that the level of free intracellular K⁺ fell markedly (from 320 mM to about 200 mM, see also Fig. 2D) during the time taken to shift the cells

into the low-K⁺ medium. Within the first minutes the total intracellular K⁺ concentration continued to decline further, and then rose for a short period (t = 5–30 min), and declined again thereafter. It is generally accepted that a significant fraction of the intracellular K⁺, referred to as the “bound” fraction, is associated with anionic macromolecules. This fraction has a much reduced osmotic and ionic activity, and can therefore be distinguished experimentally from the “free” K⁺ fraction [38]. The fraction of free intracellular K⁺ increased after a lag time, and remained at a plateau level over the next 20 min. Thereafter, this fraction decreased at a constant rate, and was barely detectable at t = 70 min. These results reveal a clear inverse correlation between *kdpFABC* transcript number and the concentration of free K⁺ ions in the cell (see Fig. 2B and D), and it is hypothesized that free intracellular K⁺ ions have a negative feedback regulatory effect on the KdpD/KdpE system.

Time-resolved dynamics of the Kdp system in a Kdp transport-defective mutant

To test this hypothesis further, we wished to analyse a mutant in which K⁺ uptake via the KdpFABC complex was compromised. For this purpose, we constructed *E. coli* strain RH010 (MG1655 *kdpA4*), which encodes a KdpFABC complex with an altered K⁺-binding site [39,40]. This strain has a chromosomal point mutation in *kdpA* (Gly345 to Ser), which replaces a glycine in the K⁺ selectivity filter III by a serine residue. Replacement of this amino acid reduces the affinity for K⁺ by about 30-fold [41]. Therefore, this mutant has very little capacity to transport K⁺ under conditions of K⁺ limitation. The strain also carries a chromosomal point mutation in the *rpsL* gene, which confers streptomycin resistance and was used for selection during strain construction [40]. Earlier tests had indicated that this mutation has no effect either on *kdpFABC* transcription or KdpFABC synthesis (data not shown).

E. coli RH010 cells were subjected to the same severe K⁺ limitation as the wild type strain. In these cultures the extracellular K⁺ concentration also decreased over time, but at a much lower rate relative to the wild type (Fig. 2E), probably due to the low activity of the KdpFABC-G345S complex. It should be mentioned that *E. coli* RH010 grows slowly under these conditions. The peak concentration of free intracellular K⁺ reached in the mutant was only half that seen in the wild type (Fig. 2H). In contrast, the initial burst in the synthesis of *kdpFABC* transcripts attained a plateau that was about three-fold higher than in the wild type (Fig. 2F). Thus, unlike the case in wild type, the time-course of *kdpFABC* transcription in the mutant follows a hyperbolic curve.

Although the mutant produced three times as many transcripts, the maximal number of KdpFABC molecules reached in the RH010 strain was only 1.5-fold higher than in wild type (Fig. 2G). To clarify the reasons for this discrepancy, pulse-chase experiments using [³⁵S]methionine were performed to compare the stability of the wild type and mutant KdpFABC complexes (Fig. S1). The half-lives of the KdpFABC complex and its KdpFABC-G345S derivative were found to be 36.7 min and 28.4 min, respectively, indicating that the mutant complex is indeed less stable than the wild type.

To probe the relationship between intracellular K⁺ and *kdpFABC* expression further, we introduced a second high-affinity K⁺ uptake system into *E. coli* RH010. The strain was transformed with plasmid pKT84 encoding the high-affinity KtrAB system from *Vibrio alginolyticus* [42] (the K_M-value of KtrAB is in the μM-range as for KdpFABC), and the transformants were treated and analysed as before. Because expression of *ktrAB* is constitutive, *E. coli* RH010 cells producing KtrAB

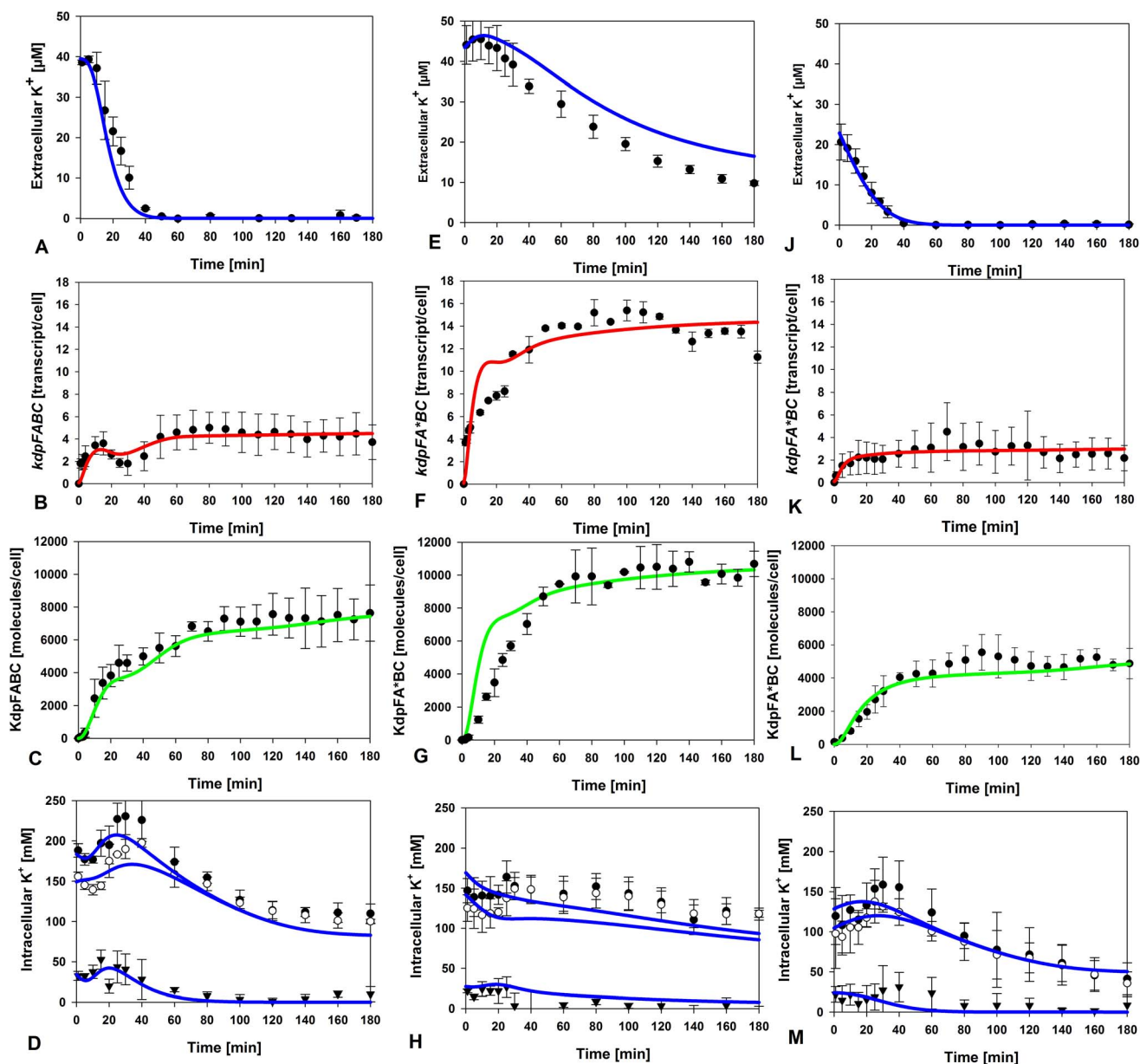


Figure 2. Induction kinetics of the Kdp system in *E. coli*. Exponentially growing cells were shifted to limiting K⁺ (40 μM K⁺) at time 0. At the indicated times thereafter cells were harvested, and extracellular and intracellular K⁺ concentrations were determined by atomic absorption spectroscopy, *kdpFABC* expression was measured by qRT-PCR, and KdpFABC production by quantitative Western blot analysis. Three different strains were used: MG1655 (A–D), RH010, which expresses KdpFA(G345S)BC and is defective in K⁺ transport (E–H), and RH010 transformed with plasmid pKT84, which encodes the high-affinity K⁺ transport system KtrAB (J–M). (A, E, J) Extracellular K⁺ concentration; (B, F, K) *kdpFABC* transcripts; (C, G, L) KdpFABC proteins; (D, H, M). Intracellular K⁺ concentrations: K⁺_{total} (●), K⁺_{bound} (○), K⁺_{bound,r} and K⁺_{free} (▼). Results of simulations based on the model are presented by the coloured lines: K⁺ concentrations (blue), transcripts (red), KdpFABC proteins (green). All experimental data are average values of at least three independent experiments, and error bars represent the standard deviation of the mean. doi:10.1371/journal.pone.0089671.g002

consumed the supply of extracellular K⁺ much faster than the wild type, which is indicated by a significant drop of the extracellular K⁺ concentration in the initial phase (Fig. 2J). For reasons that remain unclear, however, the total concentration of intracellular K⁺ immediately after the shift was lower than in the wild type (Fig. 2M). Importantly, the numbers of *kdpFABC* transcripts and KdpFABC complexes per cell at steady state were comparable to those seen in the wild type (Fig. 2K, 2L), again indicating a negative feedback effect of internal K⁺ on KdpD/KdpE activation. However, the dynamics of *kdpFABC* transcription of the

trans-complemented RH010 mutant differed from the wild type (compare Fig. 2B and Fig. 2K). The discrepancy can be explained by the fact that expression of *ktrAB* is constitutive.

In summary, the time-resolved dynamics of *kdpFABC* transcripts and KdpFABC complexes differ significantly in *E. coli* wild type and mutant RH010. Overall, the data argue for negative feedback regulation by free intracellular K⁺ under severe K⁺ limitation, which modulates KdpD/KdpE phosphorylation and thus affects *kdpFABC* expression.

Design of an extended mathematical model

The phosphorylation state of the response regulator KdpE is directly controlled by the enzymatic activities of the cognate sensor kinase KdpD [21]. Having demonstrated that the intracellular K⁺ concentration influences *kdpFABC* expression under severe K⁺ limitation, we were interested in determining the effect of K⁺ on KdpD/KdpE phosphorylation over the whole environmental induction range (0.04–2 mM K⁺). As the enzymatic reactions involved occur too rapidly for experimental investigation *in vivo*, we used mathematical modelling to address this issue. First we had to extend the existing model of the Kdp system [36], taking the experimental data obtained for the wild type and the RH010 mutant into account. Thus, we added mass balance equations to describe the temporal alterations in external [K⁺] and intracellular K⁺ concentrations (free and bound) as well as the total cell volume in our samples. The detailed derivation of the full model is set out in Materials and Methods. The relevant intracellular state variables in the model are concentrations, and thus depend on the volume of viable cells present at any given point. Potential alterations in cytoplasmic volumes were analysed over time, but the differences between stressed (40 μM K⁺) and non-stressed (10 mM K⁺) cells were found to be marginal (Table S1). An experimental comparison between total and viable cell numbers after exposure to K⁺ limitation revealed that approximately 60% of the cells survived the shift and continued to grow (Table S1). Similar values were obtained for mutant RH010 (data not shown).

The mathematical model was then used to study how K⁺ levels influence KdpD/KdpE activation and thus transcription of the *kdpFABC* operon. Since the level of phosphorylated KdpE and, consequently, the number of *kdpFABC* transcripts, seems to be a measure of the K⁺ concentration, it can be assumed that K⁺ (external or internal, Fig. 1, options **A** or **B**) either inhibits the kinase or activates phosphatase activity of KdpD (Fig. 1, options **a** or **b**). One can deduce several possible network topologies from these considerations: (i) external K⁺ (K⁺_{ex}) inhibits KdpD autophosphorylation; (ii) free intracellular K⁺ (K⁺_{free}) inhibits KdpD autophosphorylation; (iii) K⁺_{ex} enhances dephosphorylation of KdpE-P, or (iv) K⁺_{free} enhances dephosphorylation of KdpE-P. Moreover, these effects may act in combination: (i) K⁺_{ex} inhibits the kinase activity and K⁺_{free} enhances the phosphatase activity of KdpD, or (ii) vice versa. Therefore, we generated several model variants (with standard parameters from the original model and from the literature) that depicted these different network topologies and tried to calibrate them against the experimental data for the wild type and the RH010 mutant strain (Fig. 2A–H). We then used computer simulations to infer which of the conceivable networks most faithfully reproduced the experimental data. We found that the experimentally observed non-monotonic dynamic behaviour of *kdpFABC* transcription could best be explained by a positive feedback effect of the free intracellular K⁺ on the dephosphorylation of KdpE-P, i.e. K⁺ activates the phosphatase activity of KdpD. This variant yielded the best quantitative match between experimental and simulated data. Hence, in the following, the term “the model” always refers to this topology. All other topology variants tested were far less successful in reproducing the experimental data.

This finding is quite realistic for the following reasons. On the one hand, our simulations showed that KdpD/KdpE could not respond fast enough to the changes in both external and intracellular K⁺ pools if the control operated at the level of autophosphorylation alone. Furthermore, the maxima and minima of the experimentally determined time-courses of K⁺_{free} and *kdpFABC* transcripts are inversely correlated. In contrast,

external K⁺ is decreasing at a constant rate, so that this parameter is unlikely to drive non-monotonic transcript dynamics.

Finally, the model parameters had to be tuned to replicate the data reported above for wild type and the RH010 mutant strain (Fig. 2A–H), i.e. to adequately reproduce the temporal behaviour of the *kdpFABC* transcripts, the KdpFABC complexes and the different K⁺ pools (external, free and bound intracellular). Initial calibration was performed by manual adjustments made by the modeller during the simulations to improve the fit to the experimental data (see Materials and Methods). Fine-tuning of the parameters was then done using SensSB software [43], a Matlab (www.mathworks.com) toolbox that integrates different methods for sensitivity analysis and parameter estimation of dynamic models. All parameters used are summarized in Table 1.

The final model faithfully reflected the experimental data for K⁺_{free} at early time points (t = 0–40) after the shift to K⁺ limitation for the RH010 mutant, which showed a nearly 2-fold decrease in K⁺_{free} compared to the wild type (Fig. 2D and H). At later time points, however, the simulations did not predict the complete depletion of K⁺_{free} observed experimentally in the mutant. It is important to note that conditions directly after the onset of stress determine the transcription level of *kdpFABC*. Furthermore, an extremely low rate of transport by KdpFA(G345S)BC, or other unknowns which could not be implemented in the model, might influence the K⁺_{free} pool.

Simulation of KdpD/KdpE activation in response to varying external K⁺ concentrations

Our mathematical model was designed and calibrated to describe the response of the Kdp system under severe K⁺ limitation. However, we also tested the capacity of the model to qualitatively reflect the response of the *in vivo* system to a broad range of extracellular K⁺ concentrations. With increasing K⁺ availability the constitutive K⁺ uptake system Trk is expected to become more important, and therefore an uptake rate term for this transporter had to be included in the model (see Materials and Methods). Moreover, we assumed that the rate of K⁺ uptake by KdpFABC uptake rate depends on the concentration of free intracellular K⁺ (see Materials and Methods); that is, elevated levels of K⁺ will decrease the uptake velocity. This assumption is reasonable since K⁺ is transported into the cell against its concentration gradient. The values of the parameters introduced with these modifications were chosen empirically to match the experimental data (Table 1).

The model was then used to predict the quantitative behaviour of *kdpFABC* transcripts, KdpFABC complexes and the different K⁺ pools at various levels of K⁺ availability, ranging from severe K⁺ limitation to abundance. Initial levels of extracellular K⁺ (K⁺_{ex}(0)) were varied from 0.04 to 8 mM. Figure 3 depicts the results of the respective simulations. The transcript numbers (Fig. 3A) followed a non-monotonic time-course over a wide range of K⁺_{ex} concentrations, whereas numbers of KdpFABC complexes (Fig. 3B) increased monotonically over time.

The number of KdpFABC molecules predicted to be present 3 h after exposing the cells to the different external K⁺ concentrations (Fig. 3B) was plotted against the external K⁺ concentration (Fig. 4). In parallel, the corresponding experimentally determined numbers were inserted into the same plot (Fig. 4). A clear dependence was found between the number of KdpFABC molecules per cell and the external K⁺ concentration, which reflected the experimentally determined values quite well. Remarkably, the best fit was achieved at severe K⁺ limitation (0.02 to 0.1 mM K⁺), whereas under moderate (0.1 to 2.1 mM) or higher K⁺ concentrations (>2.1 mM), the model captured the

Table 1. Optimized parameters of the mathematical Kdp model.

Parameter name	Value			Units	Description
	Wild type	<i>E. coli</i> RH010	<i>E. coli</i> RH010/pKT84		
<i>Two-component system</i>					
k_1	0.23			$\frac{1}{h \cdot \mu M}$	Autophosphorylation of <i>D</i> , forward reaction rate constant
k_{-1}	5.1×10^{-6}			$\frac{1}{h \cdot \mu M}$	Autophosphorylation of <i>D</i> , backward reaction rate constant
k_2	2.27×10^3			$\frac{1}{h \cdot \mu M}$	Phosphotransfer to <i>E</i> , forward reaction rate constant
k_{-2}	8.7×10^{-4}			$\frac{1}{h \cdot \mu M}$	Phosphotransfer to <i>E</i> , backward reaction rate constant
$k_{3,f}$	40.6×10^{-3}			$\frac{1}{h \cdot \mu M^2}$	Dephosphorylation of E^P by <i>D</i>
$K_{I,D}$	520			mM	Inhibition of autophosphorylation of <i>D</i> by free K ⁺
<i>Transcription</i>					
K	4×10^4	1.2×10^4	6×10^4	1	Equilibrium binding constant of σ -factor and RNA polymerase to DNA
K_E	5.32×10^{-2}			$\frac{1}{\mu M}$	DNA-binding of free E^P , equilibrium dissociation constant
α	2.59×10^{-3}			1	Affinity factor
k_{tr}	1.06×10^4			$\frac{1}{h}$	Transcription rate constant
k_z	21.74			$\frac{1}{h}$	Transcript degradation rate constant
<i>Translation</i>					
k_{t1}	5.4			$\frac{1}{h}$	Translation rate constant of <i>D</i>
k_{t2}	162			$\frac{1}{h}$	Translation rate constant of <i>E</i>
k_{t3}	8.1×10^3			$\frac{1}{h}$	Translation rate constant of <i>F</i>
$k_{d,F}$	4.8	11.4	4.8	$\frac{1}{h}$	Degradation rate constant of <i>F</i>
k_d	0.2			$\frac{1}{h}$	Degradation rate constant of <i>D</i> and <i>E</i>
<i>Potassium pools</i>					
k_{Kdp}	7.86×10^3	0.46×10^3		$\frac{1}{h}$	K ⁺ uptake rate constant; given that $F \approx 7500 \frac{\text{proteins}}{\text{cell}}$ at steady state and cell dry weight is $DW = 2.8 \times 10^{-13}$ g, one obtains an estimate of $V_{\max} = 5.83 \frac{\mu\text{mol}}{\text{g} \cdot \text{min}}$; in the literature we find $V_{\max} = 150 \frac{\mu\text{mol}}{\text{g} \cdot \text{min}}$ [56]
$K_{M,Kdp}$	3.83	4		mM	Half saturation constant of K ⁺ uptake; literature value for Kdp: $K_M = 2 \mu\text{M}$
$K_{I,Kdp}$	100	0		mM	Inhibition of K ⁺ uptake by free K ⁺
$V_{\max,Trk}$	36.5			$\frac{\text{mmol}}{\text{h} \cdot \text{l}}$	Maximum velocity of K ⁺ uptake by Trk
$K_{M,Trk}$	0.1			mM	Half saturation constant of K ⁺ uptake by Trk
$V_{\max,Ktr}$	0		400	$\frac{\text{mmol}}{\text{h} \cdot \text{l}}$	Maximum velocity of K ⁺ uptake by KtrAB
$K_{M,Ktr}$	0		5×10^{-2}	mM	Half saturation constant of K ⁺ uptake by KtrAB;
$V_{\max,lys}$	1×10^{-2}	2×10^{-2}	1×10^{-2}	$\frac{\text{mmol}}{\text{h} \cdot \text{l}}$	Maximum K ⁺ release rate due to cell lysis
$K_{M,lys}$	150			mM	Half saturation constant of K ⁺ release due to cell lysis
k_{bind}	8			$\frac{1}{h}$	Binding rate constant of free K ⁺
$K_{M,free}$	250			mM	
k_{diss}	7.81			$\frac{1}{h}$	Dissociation rate constant of bound K ⁺
τ	0	0.35	0	h	"Delay" constant for intracellular K ⁺ exchange

Table 1. Cont.

Parameter name	Value			Units	Description
	Wild type	<i>E. coli</i> RH010	<i>E. coli</i> RH010/pKT84		
<i>Growth</i>					
$k_{\mu,1}$	0.54	0.59	0.54	$\frac{1}{h}$	Maximum growth rate
$k_{\mu,2}$	1.43×10^{-3}	1.52×10^{-3}	1.57×10^{-3}	$\frac{1}{l}$	Carrying capacity, inflection point of growth curve
n	6	1	6	1	Determines maximum steepness of growth curve

The experimental data for the wild type, the RH010 mutant and the RH010/pKT84 mutant cannot be reproduced using a single set of parameters. The Table lists the values of each parameter used to describe the dynamics of each strain.
doi:10.1371/journal.pone.0089671.t001

decrease in KdpFABC production qualitatively but not quantitatively (Fig. 4).

We also predicted the time-courses of free and bound K⁺ (Fig. 3C, D). Under extreme K⁺ limitation, uptake of the residual external K⁺ initially out-weights dilution by cell growth. Then the residual cell growth becomes the dominant factor, while at high external K⁺ concentrations (1–8 mM), K⁺ uptake constantly compensates for dilution of the internal K⁺ pools by cell growth.

The model was also used to simulate and predict the concentrations of phosphorylated KdpD and KdpE at the various external K⁺ concentrations. Since experimental determination of KdpD and KdpE phosphorylation kinetics *in vivo* is not possible thus far, the simulations can be seen as virtual measurements. Both KdpD-P and KdpE-P exhibited non-monotonic time-courses for all initial K⁺_{ex} concentrations (Fig. 3E, F).

Discussion

In natural environments bacteria are often exposed to long-lasting periods of stress. Hence, not only must they be capable of adapting rapidly to changing conditions, they must also be able to cope with persisting stress conditions. With this consideration in mind, we quantitatively analysed and simulated the dynamics of the *E. coli* Kdp system over a period of 3 h after activation.

When *E. coli* is exposed to limiting K⁺ concentrations, the KdpD/KdpE signalling cascade is instantly activated and, consequently, *kdpFABC* transcription is rapidly induced. After a lag period required for its synthesis and assembly, the KdpFABC complex then mediates high-affinity K⁺ uptake. Thus *kdpFABC* expression was turned on immediately after shifting wild type *E. coli* cells into medium containing a very low level of K⁺ (40 μM), reached a peak in less than 20 min, and then declined before rising again at 30 min. This transient dip points to negative feedback regulation of *kdpFABC* transcription, which was predicted in our earlier *in silico* and *in vivo* studies, and was also observed in an independent study [32,36]. Negative feedback regulation is frequently employed during stress-dependent processes in bacteria to save energy for mRNA synthesis [44]. By monitoring our cultures for a longer time period, we found that shortly after the first induction peak, the concentration of free intracellular K⁺ falls significantly, and the cells essentially run out of K⁺ once more. It is important to note that this loss of K⁺ is attributed to the onset of growth. Consequently, the KdpD/KdpE signalling cascade and *kdpFABC* transcription are activated for a second time. At this stage, the level of *kdpFABC* expression begins to rise again to meet the cell's significantly increased need for K⁺. Thereafter (t = 60 min) a steady state is attained, marked by continued

transcription of *kdpFABC* and synthesis (and very probably turnover) of KdpFABC, cell division and cell lysis, with concomitant release and re-uptake of K⁺. Note that, over the whole time-course, the extracellular K⁺ concentration decreased at a constant rate, and was clearly uncoupled from KdpFABC production and hence from KdpD/KdpE activation.

The observed pattern of KdpFABC production, and the known inhibitory effect of K⁺ on KdpD/KdpE phosphorylation *in vitro* [29–31], provide clues to the nature of the primary stimulus for KdpD phosphorylation. It is conceivable that due to the shift of cells into a low-K⁺ environment, the ion's inhibitory effect on the phosphorylation of KdpD/KdpE is relieved. Specifically, according to our simulations, inhibition of the phosphatase activity of KdpD is required to keep KdpE in the phosphorylated state and enable high-level production of KdpFABC, which in turn increases the amount of free K⁺ in the cell. Our calculations indicated that this increase in the concentration of free intracellular K⁺ enhances KdpD phosphatase activity and thus reduces the concentration of phospho-KdpE. This is the first indication of an inverse correlation between KdpD/KdpE phosphorylation and the concentration of free intracellular K⁺.

The hypothesis that the intracellular K⁺ concentration modulates KdpD/KdpE phosphorylation is further supported by our finding that no hint of negative feedback regulation is observed when the KdpFABC transport-defective *E. coli* mutant RH010 is subjected to similar K⁺ limitation. Moreover, the expression profiles in the RH010 mutant also argue against an effect of the extracellular K⁺ concentration on KdpD/KdpE activation under these conditions. Thus, although - due to the defect in K⁺ uptake by the mutant KdpFABC complex - the extracellular K⁺ concentration declines more slowly than in case of the wild type, levels of *kdpFABC* transcripts rise to far higher levels. Notably, *trans*-complementation of this *E. coli* mutant by the high-affinity KtrAB K⁺ transporter from *V. alginolyticus* reduced *kdpFABC* expression to a level comparable to that in wild type. The experimentally determined and theoretically modelled data for the non-complemented mutant strongly support the notion that the intracellular K⁺ concentration is an important modulator of KdpD/KdpE activities under conditions of severe K⁺ limitation. Concomitantly, these results throw light on the mode of negative feedback regulation [36] by which the uptake of K⁺ by the KdpFABC complex down-regulates its own expression. Regulation of KdpD/KdpE phosphorylation by the intracellular K⁺ concentration is in line with earlier observations which indicated that both extracellular Cs⁺ and low pH significantly reduce the availability of free intracellular K⁺ and lead to induction of *kdpFABC* expression [27,28].

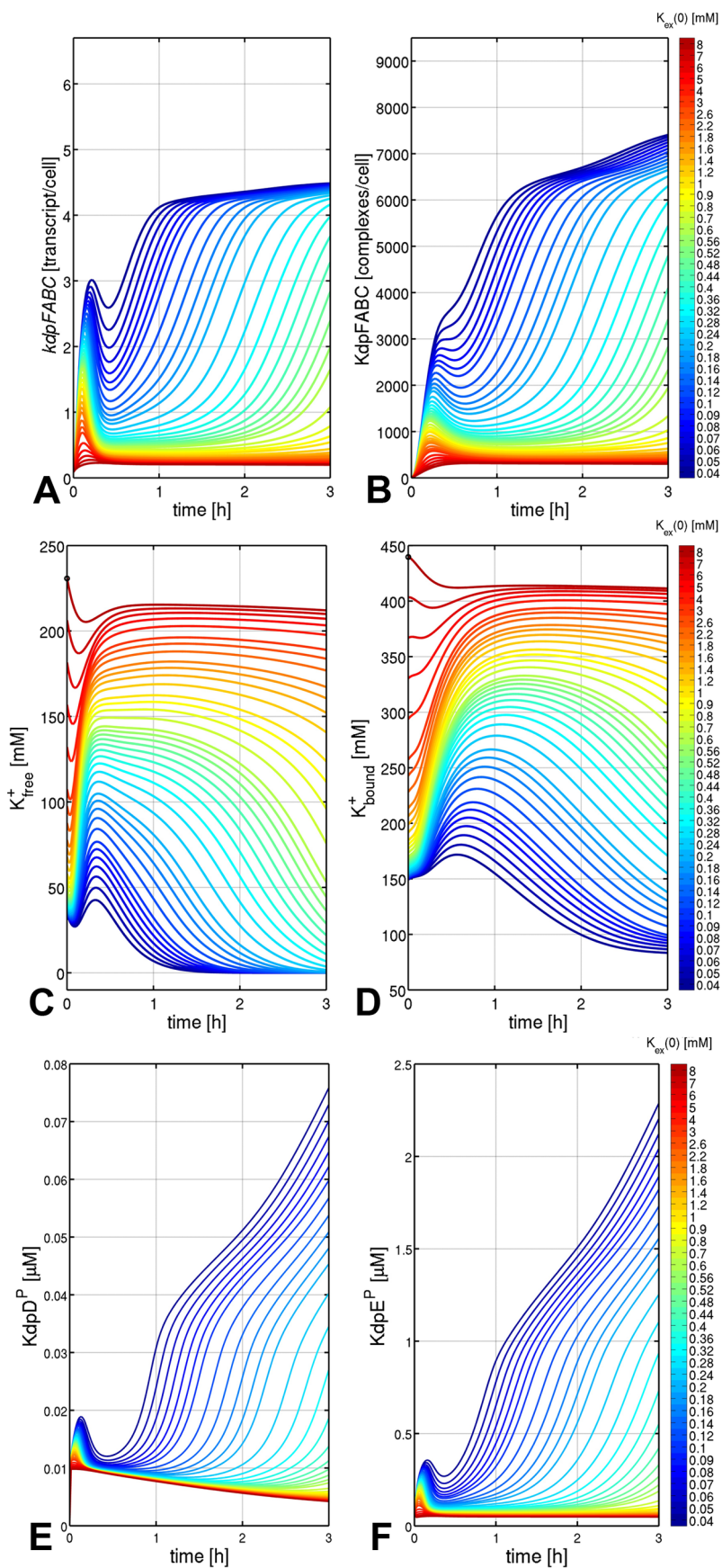


Figure 3. Predicted time-courses of intracellular variables of the Kdp system derived from simulations based on the model for different levels of K⁺ availability. K⁺ availability is determined by the initial concentration of external K⁺ at t = 0 h, K⁺_{ex(0)}. *kdpFABC* transcripts and KdpFABC complexes decrease with increasing K⁺_{ex} levels (A, B). Intracellular K⁺ (free and bound) increases with increasing external K⁺ (C, D). Time-courses of phosphorylated KdpD and KdpE are qualitatively very similar to the *kdpFABC* curves (E, F). doi:10.1371/journal.pone.0089671.g003

However, *kdpFABC* expression, and therefore KdpFABC production, is not only induced at very low external K⁺ concentrations (below 0.1 mM), but gradually increases at moderate K⁺-limiting conditions (2 to 0.1 mM) [22,23,32]. Our simulations very well captured this phenomenon, too (Fig. 3A, B, Fig. 4). Though, the simulations perfectly reproduced the experimental data at K⁺ concentrations below 0.1 mM, but deviated from them under moderately K⁺-limiting conditions (0.1 to 2 mM) and non-stress conditions (above 2.1 mM) (Fig. 4).

Therefore, it is suggested that the internal K⁺ pool predominantly acts as primary stimulus under extreme K⁺ limitation, and that external K⁺ influences KdpD/KdpE activation under moderate stress conditions, when a significant drop in the intracellular K⁺ concentration is unlikely (Figs. 3C and 3D). This proposal is in accord with recent findings by Altendorf and coworkers, who suggest that KdpD senses the external K⁺ concentration as one stimulus [32]. Nevertheless, this hypothesis needs further experimentation since evidence for a periplasmic K⁺-binding site is lacking, and it is unclear whether external K⁺ influences the kinase or the phosphatase activity of KdpD.

During modelling it emerged that the response of the RH010 mutant that produces an inactive KdpFABC was hampered by the fact that the ratio of transcript to protein at steady-state differed from the values for the wild type strain. By means of sensitivity analysis, one parameter (*K*) could be identified which lumps

together several kinetic constants for transcription initiation. After re-estimation the accuracy could be improved. It is likely that the Kdp system is not only controlled at the transcriptional level, but also at the post-translational level by proteolysis, and at the activity level [26]. Whether post-translational regulation is linked to K⁺ is unclear.

In summary, our study reveals that the tight interplay between theory and experiment greatly helps to improve our understanding of bacterial sensing and signalling pathways. Moreover, it also highlights how important it is to record the time-dependent input/output ratios of these systems. Lastly, this is one of the rare examples demonstrating the bacterial dynamics during the management of prolonged stress.

Materials and Methods

Materials

[γ -³²P]ATP and [³⁵S]methionine were purchased from GE Healthcare (Munich), and ³H₂O and [¹⁴C]sucrose were obtained from Biotrend (Cologne). SYBR Green Mix was from BioRad (Munich), the DyNAmoTM cDNA Synthesis Kit and Protein A magnetic beads were from New England Biolabs (Frankfurt am Main). Goat anti-(rabbit IgG)-alkaline phosphatase was obtained from Biomol (Hamburg). Purified KdpFABC protein was supplied by Marc Bramkamp (Osnabrück University). RNase-free deoxyribonuclease I was from Fermentas (St. Leon-Rot), and silicone oil (DC550) was from Serva (Heidelberg). All other reagents were reagent grade and obtained from commercial sources.

Strains and plasmids

E. coli strains MG655 (wild type K-12 strain) [45], MG1655 *rpsL150* [40], and *E. coli* RH010 (MG1655 *rpsL150 kdpA4*) [40] were used for these studies. *E. coli* RH010 is characterized by a chromosomal point mutation in *kdpA* (G1033A), which leads to the replacement of the glycine at position 345 in KdpA by serine, and results in a KdpFABC complex that is defective in K⁺ transport. Plasmid pKT84 [42] encodes *ktrAB* under the control of its native promoter.

Measurement of *kdpFABC* expression by quantitative RT-PCR

Transcription of *kdpFABC* under K⁺ limitation was monitored by quantitative RT-PCR (qRT-PCR). *E. coli* MG1655, *E. coli* MG1655 *rpsL150* and *E. coli* RH010 (MG1655 *rpsL150 kdpA4*) were aerobically grown in phosphate-buffered minimal medium containing 10 mM K⁺ [46] until the mid-exponential growth phase and then shifted to fresh, pre-warmed medium containing 40 μ M (K⁺ limitation) by filtration. Cultivation was continued at 37°C. For cultivation of *E. coli* RH010 pKT84, the medium was supplemented with 100 μ g \times ml⁻¹ ampicillin. At the times indicated, samples were taken from the cultures, and total RNA was isolated using acidic phenol/chloroform [47]. Contaminating genomic DNA was removed by DNase digestion (DNase I, RNase-free, Fermentas). Aliquots (4 μ g) of total RNA were subjected to reverse transcription using the RevertAidTM First Strand cDNA Synthesis Kit (Fermentas) and an oligo (dt)₁₈ primer, and the resulting cDNA was used for subsequent quantitative real-time

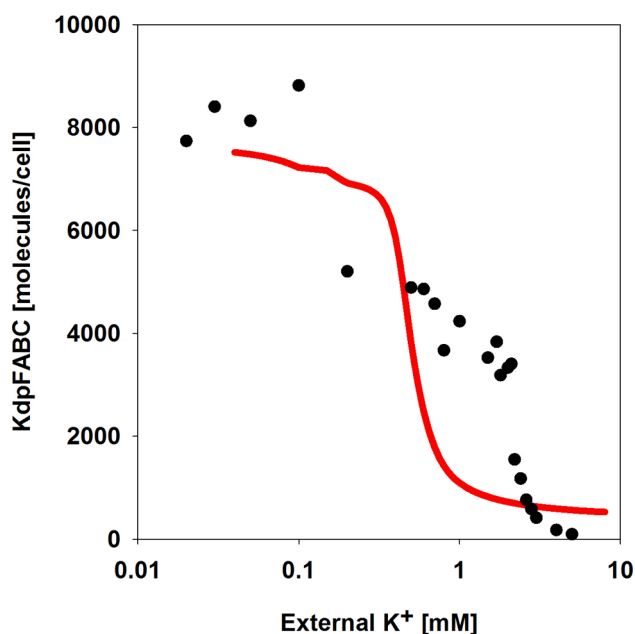


Figure 4. Relationship between the level of KdpFABC at steady state and the initial external K⁺ concentration. Cells were grown in minimal medium containing 10 mM K⁺, then shifted in the mid-logarithmic growth phase to the indicated external K⁺ concentrations (40 μ M–5.0 mM K⁺), and after 3 h of aerobic incubation at 37°C, cells were harvested, and the level of KdpFABC was determined by quantitative Western blot analysis (●). The red trace depicts the relationship predicted by the model. doi:10.1371/journal.pone.0089671.g004

PCR. qRT-PCR was conducted on an iQ5 Multicolor Real-Time PCR Detection System (BioRad) using the Maxim SYBR Green/ROX qPCR Master Mix (BioRad) and analysed with the iQ5 Optical System Software (BioRad). *kdpA* was amplified by qPCR using primers 5'-CCAACCGCACTGACCAACTTC-3' and 5'-TCGCCATCACTTCACCAAAG-3'. *recA* was used as the reference gene. Prior to qPCR procedure, all samples were heated for 3 min at 95°C, and then taken through 40 cycles of 10 s at 95°C and 30 s at 65°C. Binding of the primers for the qPCR and amplification of the appropriate single PCR product corresponding to the *kdpA* gene were checked by melting-curve analysis and gel electrophoreses. All reactions were performed on three biological replicates and the transcript amount was calculated using the $\Delta\Delta C^t$ method [48].

Determination of extracellular and intracellular K⁺ concentrations

K⁺ concentrations were determined by atomic absorption spectroscopy [49]. Briefly, 1-ml samples taken from a growing *E. coli* culture were centrifuged through 200 μ l silicone oil (DC550; 1:10 diluted with hexadecane) for 2 min at 13,000 rpm. The K⁺ content of the cell pellets and the supernatants were determined in an atomic absorption spectrometer (Varian AA240 Spectroscopy Instrument, Agilent Technologies, Böblingen). To determine the fraction of bound and freely diffusible K⁺, duplicate 0.5-ml samples were collected and centrifuged. Cell pellets were resuspended in either 0.5 ml medium (total K⁺) or 0.5 ml ddH₂O (bound K⁺) [49]. After centrifugation through silicone oil, the K⁺ content of the cell pellets was determined by atomic absorption spectrometry. The fraction of free K⁺ is defined as the difference between the total K⁺ content and the bound K⁺ content. The intracellular concentrations were calculated by taking the number of cells per sample and the cytoplasmic volumes into account. Since cell volumes were found to remain more or less constant during the experiments (Table S1), an average value of 8.12×10^{-16} l per cell was used in all calculations.

Determination of cytoplasmic volume

The size of the cytoplasmic water space can be used as a proxy for the cytoplasmic volume [50], and was determined as described by Altendorf and coworkers [23]. Since [¹⁴C]sucrose cannot be metabolized by *E. coli* MG1655 (as shown previously) and therefore does not enter the cytoplasm, in contrast to ³H₂O, the cytoplasmic volume could be calculated by determining the difference between their distributions, taking their nuclide content into account. Briefly, ³H₂O (1 mCi/ml) and [¹⁴C]sucrose (0.1 mCi/ml, glucose-free, ubiquitously labelled) were added to 1.3-ml samples of growing *E. coli* cells. After 1 min, cells were centrifuged for 2 min through a 200- μ l silicone oil layer of appropriate density (see above). The cell pellets were separated from the supernatants, and cells were lysed by treatment with 1 ml 0.4 M NaOH at 62°C for 1 h. The radioactivity of the two labelled compounds in the cell pellet was quantified simultaneously by liquid scintillation counting. The dual-label protocol was used so the original counts per minute of each nuclide could be converted into disintegrations per minute (dpm) taking the overlap of the energy distribution spectra of the two nuclides into account. For quantification, the radioactivity present in 50 μ l of supernatant was also determined. As ³H₂O penetrates into every part of the cell, the total cellular water space including the extracellular water layer was calculated as follows: (³H dpm of the pellet) \times 50 μ l/³H dpm of 50 μ l supernatant). Since [¹⁴C]sucrose is only excluded from the cytoplasm, the volume of the extracellular water

layer plus the periplasmic space was calculated as follows: (¹⁴C dpm of the pellet) \times 50 μ l/(¹⁴C dpm of 50 μ l supernatant).

The difference between the space occupied by ³H₂O and the space occupied by [¹⁴C]sucrose gives the volume of cytoplasmic water, which includes all water layers bound to biological surfaces, the so-called bound water [51,52], as well as the freely diffusing water, the so-called bulk water. The water space of the cytoplasm is referred to as the cytoplasmic volume, which does not encompass the volume of all macromolecules in the cytoplasm. The concentration of cytoplasmic solutes was calculated on the basis of the cytoplasmic volume.

Determination of KdpFABC production by quantitative Western blot analysis

Levels of KdpFABC in *E. coli* strains were determined by quantitative Western blot analysis. The respective *E. coli* strains were grown as described above. At the time points indicated, aliquots of the cultures were removed and the cells were collected by centrifugation, resuspended in SDS sample buffer and subjected to SDS-PAGE [53]. Known concentrations of purified KdpFABC were used to obtain a standard curve, and 0.1 μ g of purified KdpFABC was also loaded onto each gel as a standard. Coomassie Blue staining of separate gels verified loading of equal amounts of protein. Proteins were then electro-blotted onto a nitrocellulose membrane, and the blots were blocked with 5% (w/v) skim milk in buffer A (10 mM Tris/HCl pH 7.4, 0.15 M NaCl) for 1 h. Anti-KdpB antibody [30] was added at a final dilution of 1:10,000 and incubation was continued for 1 h. After washing with buffer A, goat anti-(rabbit IgG) conjugated with alkaline phosphatase was added in a final dilution of 1:2,500, and incubation was continued for 1 h. After washing thoroughly, blots were developed with substrate solution [50 mM NaCO₃, pH 9.5, 0.01% (w/v) nitro-blue-tetrazolium, 5 mg/ml 5-bromo-4-chloro-3-indolylphosphate]. Blots were scanned at high resolution in 256 grey scales and imported as TIF files into ImageQuant 5.0, and the amount of KdpB was quantified by comparison with the standard curve.

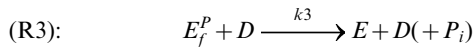
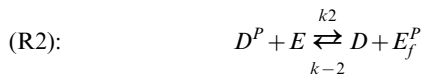
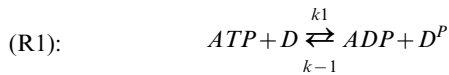
In vivo protein stability assay

The stability of KdpFABC under K⁺ limitation was analysed *in vivo* in *E. coli* MG1655 *rpsL150* and *E. coli* RH010 (MG1655 *rpsL150 kdpA4*) by labelling the complex with [³⁵S]methionine. Cells were grown to exponential phase and shifted to K⁺ limitation as described above. After 10 min, 2.5 μ Ci/ml (final concentration; 1000 Ci/mmol) [³⁵S]methionine was added, and cells were incubated for an additional 10 min to allow uptake of label into *de novo* synthesized proteins, in this case predominantly the subunits of the KdpFABC. Then, non-radioactive methionine was added in excess (2 mM final concentration) to block further radiolabeling of nascent proteins. After different times 1-ml culture aliquots were collected, and immediately frozen in liquid nitrogen to stop protein biosynthesis. Before detection of radiolabeled KdpFABC, the protein was concentrated using immunomagnetic separation. For this purpose, cells were sonified (3 \times 30 sec, interrupted by 30-sec breaks, 50% magnitude) and proteins were solubilized with 1.5% (w/v) *n*-dodecyl- β -D-maltoside. α KdpFABC antiserum [30] containing 5 μ g protein (antibodies) was added, and samples were incubated with gentle agitation at 4°C for 1 h. Then, Protein-A-coupled magnetic beads with a total binding capacity of 10 μ g human IgG were added (25 μ l), and samples were further incubated at 4°C for 1 h. Beads were recovered by applying a magnetic field, washed three times with buffer [10 mM Tris/HCl pH 7.5, 150 mM NaCl, 1 mM EDTA, 1 mM EGTA, 0.2 mM PMSF, 1.5% (w/v) *n*-dodecyl- β -D-maltoside], and

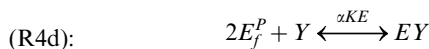
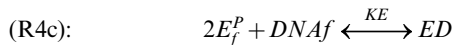
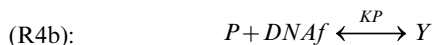
proteins were finally removed from the beads by addition of 30 μ l 3-fold concentrated SDS sample buffer [53] containing 4 M urea. Samples including a purified KdpFABC that had also been radiolabelled with ³⁵S, were then subjected to SDS-PAGE [53], stained with Coomassie Blue, and gels were dried. Radiolabeled KdpFABC was detected by autoradiography of the stained and dried gel and quantified by comparison with the signal for the standard.

Mathematical model for the Kdp system

The mathematical model of the Kdp system [36] is composed of two modules: the first module captures the interactions between KdpD and KdpE, the second describes the transcription of the target regulon *kdpFABCDE* and the synthesis of its protein products. The first module comprises the rate equations for autophosphorylation (R1) of the sensor kinase KdpD [*D*], transfer of the phosphoryl group (R2) from KdpD-P [*D*^{*P*}] to the response regulator KdpE [*E*], and the dephosphorylation (R3) of free KdpE-P [*E*^{*P*}]_{*f*} resulting in inorganic phosphate [*P*_{*i*}]:



In addition, the module describes the initiation of transcription, which depends on the interaction of polymerase and KdpE proteins with free DNA. This process can be described by the following set of reactions



These reactions comprise the binding of free polymerase [*P*_{*f*}] to free sigma factor [σ_f] (R4a), the binding of the polymerase complex [*P*] to promoter DNA [*DNA*_{*f*}] ((R4b)+(R4e)) and the binding of two free phosphorylated KdpE response regulator proteins [*E*^{*P*}]_{*f*} to their cognate binding site in the DNA ((R4c)+(R4d)). The order of binding of polymerase and response regulator is mutually independent; however the second reactant binds with a higher affinity, represented by the factor α . The parameters K_i ($i = \sigma, P, E$) denote the equilibrium dissociation constants $K_i = k_{-i}/k_i$

k_i . Reactions (R4a)-(R4e) are assumed to be very fast in comparison to protein synthesis. Therefore the rapid equilibrium approach was applied to each of the reactions, leading to a set of algebraic equations that describe the protein complexes as functions of the protein concentrations and the reaction constants:

$$P = \frac{1}{K_\sigma} P_f \sigma_f$$

$$Y = \frac{1}{K_P} P DNA_f = \frac{1}{K_\sigma K_P} P_f \sigma_f DNA_f$$

$$ED = \frac{1}{K_E} E_f^{P2} DNA_f$$

$$EY = \frac{1}{\alpha K_E} E_f^{P2} Y = \frac{1}{\alpha K_P} P ED = \frac{1}{\alpha K_E K_\sigma K_P} P_f \sigma_f E_f^{P2} DNA_f$$

We obtain the following conservation relations for the total concentration of DNA

$$DNA_0 = DNA_f + Y + ED + EY$$

and the total concentration of phosphorylated response regulator

$$E_P = E_f^P + 2ED + 2EY,$$

with

$$K = \frac{K_\sigma K_P}{P_f \sigma_f}$$

(Since experimental quantification of P_f and σ_f is almost impossible, both variables are considered to be constant and are combined in a single parameter K , together with the dissociation constants K_σ and K_P).

Thus, the mathematical description of the first module comprises two differential equations for D^P and E^P (total amount of phosphorylated response regulator, free and DNA-bound), two algebraic equations to calculate the amounts of free DNA DNA_f , and the unbound response regulator E_f^P , and two algebraic equations to determine the amount of unphosphorylated sensor kinase D and response regulator E :

$$\frac{dD^P}{dt} =$$

$$-k_{-1} D^P ADP - k_2 D^P E + k_1 D ATP \frac{K_{I,D}^3}{K_{I,D}^3 + K_{free}^+ 3} + k_{-2} D E_f^P$$

$$\frac{dE^P}{dt} = -k_{-2} D E_f^P - k_3 D E_f^P + k_2 D^P E$$

$$E^P = E_f^P + 2E_f^{P2} DNA_f \left(1 + \frac{1}{\alpha K}\right) \frac{1}{K_E}$$

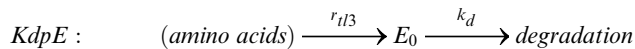
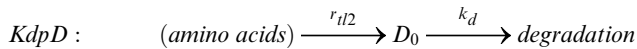
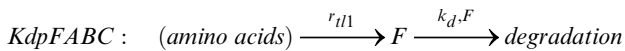
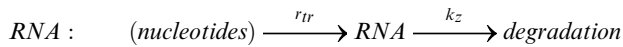
$$DNA_0 = DNA_f \left(1 + \frac{1}{K} + E_f^{P2} \left(1 + \frac{1}{\alpha K} \right) \frac{1}{K_E} \right)$$

$$D = D_0 - D^P$$

$$E = E_0 - E^P.$$

D_0 and E_0 are the total concentrations of the sensor kinase KdpD and the response regulator KdpE, respectively. The balance equations for these variables will be derived in the following. The concentration of DNA_0 is always taken to be constant.

To describe the overall module up to the level of KdpFABC [F] production, the model was extended to include a second module comprising equations for the transcript dynamics (reflecting synthesis and stability of the mRNA), and the dynamics of the proteins KdpFABC, KdpD and KdpE:



Since it is assumed that the concentration of nucleotides and amino acids is not limiting, the rate laws r_{tr} and r_{ili} ($i = 1, 2, 3$) do not depend on the monomer concentration.

Using the relations derived for the first module, transcription efficiency (i.e. relative promoter occupancy) is calculated as

$$\psi = \frac{Y + EY}{DNA_0} = \frac{1}{\alpha K + 1} \frac{\alpha K_E + E_f^{P2}}{\alpha K + 1 + E_f^{P2}}.$$

Following a method established earlier [54], the rate of mRNA synthesis r_{tr} is then calculated with the following equation:

$$r_{tr} = k_{tr} \psi DNA_0.$$

Thus, the differential equations for transcript and protein synthesis read:

$$\frac{d RNA}{dt} = k_{tr} \psi DNA_0 - (k_z + \mu) RNA$$

$$\frac{d F}{dt} = k_{il1} RNA - (k_{d,F} + \mu) F$$

$$\frac{d D_0}{dt} = k_{il2} RNA - (k_d + \mu) D_0$$

$$\frac{d E_0}{dt} = k_{il3} RNA - (k_d + \mu) E_0,$$

where F represents the K⁺ uptake system KdpFABC and μ the specific growth rate of the cells. The rate of degradation of KdpFABC is chosen to be a linear function of the protein concentration, i.e. $r_{deg,F} = k_{d,F} F$. This choice is discussed in more detail in the Results section in relation to the putative controlled proteolysis.

In the previously published model [36] the feedback effect of KdpFABC on the two-component system and its dependence on K⁺ concentration was described by a black box approach. It was assumed that an increase in the intracellular K⁺ concentration mediated by KdpFABC-dependent K⁺ uptake should promote the dephosphorylation of E_f^P (via parameter k_3). This was described by the following equation

$$k_3 = k_h \frac{F}{K_h + F'}$$

where k_h and K_h represent adjustable parameters.

In order to turn the black box model into more of a grey box, which allows a better understanding of the mechanism of K⁺ uptake by *E. coli*, detailed mass balance equations for intra- and extracellular K⁺ concentrations were included. Intracellular K⁺ is assumed to exist in two pools: One fraction is bound to macromolecules while the other is assumed to be freely diffusible in the cell.

The pools of extracellular, and free and bound intracellular, K⁺ are linked with each other: Extracellular K⁺ is taken up by viable cells and added to the pool of the free intracellular K⁺. The pools of free and bound K⁺ are connected by binding to/dissociation from macromolecules. Due to the lack of direct quantitative information on these processes, the respective kinetics was empirically chosen as

$$r_{bind} = \left(-k_{bind} K_{free}^+ + k_{diss} K_{bound}^+ \frac{K_{free}^+}{K_{M,free} + K_{free}^+} \right) \frac{t^6}{t^6 + \tau^6}.$$

This formulation ensures that free and bound K⁺ equilibrate at high K⁺ availability. The artificial delay term $\frac{t^6}{t^6 + \tau^6}$ was introduced to account for the dynamics of the free and bound K⁺ fractions in the RH010 mutant (see Fig. 2), where there is almost no exchange between free and bound K⁺ for the first 20 min. Additionally, dead cells are assumed to release K⁺ (free and bound) into the medium.

Transport processes between extracellular space and cytoplasm are modeled using a Michaelis-Menten rate law

$$r_{trans} = V_{max,trans} \frac{K^+}{K_{m,trans} + K^+}.$$

In order to account for the time-dependent variations in the number of KdpFABC complexes, the V_{max} value of the uptake rate is a function of the KdpFABC concentration:

$$V_{\max,up} = k_{up} F.$$

Depending on the respective strain, K⁺ is taken up by up to three transporters: i) In the wild type, KdpFABC and Trk are present, ii) in the RH010 mutant, a KdpFABC with reduced transport capacity and Trk are present, and iii) in the RH010 mutant carrying plasmid pKT84, a KdpFABC with reduced transport activity, Trk and the KtrAB transporter are all present. Therefore, in its most general formulation, the model comprises three different K⁺ uptake terms, one for each transporter. Besides that, there is one term to describe K⁺ efflux due to cell lysis.

In addition, we have to take into account that the extracellular K⁺ concentration is normalized with respect to the medium volume that is seen by all cells, whereas the intracellular concentrations are normalized with respect to the volume of a single cell. Therefore, in the balance equation for the extracellular K⁺ concentration, both the K⁺ uptake rate and the efflux rate due to cell lysis are proportional to the total volume of all cells. Taken together, these considerations led to a set of four additional differential equations that characterize K⁺ uptake:

$$\begin{aligned} \frac{dK_{ext}^+}{dt} &= -k_{Kdp} F \frac{K_{ext}^+}{K_{M,Kdp} + K_{ext}^+} \frac{K_{I,Kdp}^3}{K_{I,Kdp}^3 + K_{free}^+} Vol_{cells} \\ &\quad - V_{\max,Trk} \frac{K_{ext}^+}{K_{M,Trk} + K_{ext}^+} Vol_{cells} \\ &\quad - V_{\max,Ktr} \frac{K_{ext}^+}{K_{M,Ktr} + K_{ext}^+} Vol_{cells} \\ &\quad + V_{\max,lys} \frac{K_{free}^+ + K_{bound}^+}{K_{M,lys} + K_{free}^+ + K_{bound}^+} Vol_{cells} \\ \frac{dK_{free}^+}{dt} &= k_{Kdp} F \frac{K_{ext}^+}{K_{M,Kdp} + K_{ext}^+} \frac{K_{I,Kdp}^3}{K_{I,Kdp}^3 + K_{free}^+} \\ &\quad + V_{\max,Trk} \frac{K_{ext}^+}{K_{M,Trk} + K_{ext}^+} \\ &\quad + V_{\max,Ktr} \frac{K_{ext}^+}{K_{M,Ktr} + K_{ext}^+} \\ &\quad + \left(-k_{bind} K_{free}^+ + k_{diss} K_{bound}^+ \frac{K_{free}^+}{K_{M,free} + K_{free}^+} \right) \frac{t^6}{t^6 + \tau^6} \\ &\quad - \mu K_{free}^+ - V_{\max,lys} \frac{K_{free}^+}{K_{M,lys} + K_{free}^+ + K_{bound}^+} \end{aligned}$$

$$\begin{aligned} \frac{dK_{bound}^+}{dt} &= \left(k_{bind} K_{free}^+ - k_{diss} K_{bound}^+ \frac{K_{free}^+}{K_{M,free} + K_{free}^+} \right) \frac{t^6}{t^6 + \tau^6} \\ &\quad - \mu K_{bound}^+ - V_{\max,lys} \frac{K_{bound}^+}{K_{M,lys} + K_{free}^+ + K_{bound}^+} \end{aligned}$$

$$\frac{dVol_{cells}}{dt} = \mu Vol_{cells}.$$

It should be noted that it is not possible to distinguish between the free and bound K⁺ balances in viable and dead cells. Therefore, in the model the average cell takes up and releases K⁺ at the same time. Due to K⁺ limiting conditions, the growth rate μ is not constant and varies over time. This variable was modelled using the approach

$$\mu = k_{\mu,1} \left(1 - \left(\frac{Vol_{cells}}{k_{\mu,2}} \right)^n \right),$$

so that the solution of the differential equation $dVol_{cells}/dt = \mu Vol_{cells}$ corresponds to the generalized logistic function, an asymmetric sigmoid curve which provides a convenient approach for the modelling of growth of different organisms [55].

There are several alternative ways of modelling the influence of K⁺ on the KdpD/KdpE two-component system. In order to account for the non-monotonic dynamics of the *kdpFABC* transcript, K⁺ could either inhibit the autophosphorylation of KdpD or amplify/enhance the dephosphorylation of KdpE-P, or both. We modelled the possible inhibiting effect of K⁺ on the kinase activity of KdpD by taking

$$k_1 = k_{1,f} \frac{K_{I,D}}{K_{I,D} + K^+}.$$

The enhancing effect of K⁺ on the phosphatase activity of KdpD was modelled by taking

$$k_3 = k_{3,f} \cdot K^+.$$

In the final model, we assumed that an increase in the free intracellular K⁺ concentration mediated by K⁺ uptake through KdpFABC should increase the dephosphorylation of E_f^P (via parameter k_3) so that

$$k_1 = const.$$

and

$$k_3 = k_{3,f} \cdot K_{free}^+,$$

where $k_{3,f}$ represents an adjustable parameter.

For the analysis of proteolysis, the degradation of the corresponding protein [P] was modelled using the following differential equation

$$\frac{dP}{dt} = -(k_{deg} + \mu)P,$$

where k_{deg} is the degradation time constant. If protein degradation is actively controlled, k_{deg} is expected to vary under different experimental conditions. The specific growth rate μ is also time dependent; therefore it is determined using the empirical equation given above.

Model calibration

Prior to parameter estimation, parameter sensitivities and correlations needed to be analysed in order to detect potential sources of identifiability problems. Parameters that show very little sensitivity compared to others, as well as correlations among parameters (which would indicate that only combinations of parameters, rather than single ones, can be identified), can lead to

far-from-optimal results (the theoretical foundations of this topic are beyond the scope of this study, therefore we refer the reader to [43] and the references therein).

Several parameters that determine the dynamics of the two-component system (k_{-1} , k_2 , k_{-2}) showed very little sensitivity and were highly correlated with each other. Therefore, these parameters are virtually unidentifiable and could be set to nominal values, and were therefore excluded from parameter estimation. The parameters describing the release of K⁺ due to cell lysis and the synthesis of the proteins KdpD and KdpE also showed low sensitivities. In addition, we found high correlations among the parameters describing the transcription of *kdpFABC*.

In order to describe and reproduce the experimental data for the RH010 mutant, the wild type model was used, albeit with appropriate adjustments of several parameters. To account for the lower rate of K⁺ uptake, the value of the parameter k_{Kdp} was changed (Table 1). Furthermore, the increase in transcripts/cell in this mutant was greater than in the wild type. By means of sensitivity analysis of the model this observation could theoretically be explained by changes in each of the parameters that describe transcription efficiency and transcript synthesis, i.e. α , K_E , K , DNA_0 and k_{tr} . Sensitivity analysis revealed that parameter K has a strong impact on the steady-state level; therefore, this parameter was adjusted accordingly. K is a lumped/aggregated parameter that contains several variables, namely the (unknown) concentrations of the sigma factor and polymerase, as well as the equilibrium constants for the reactions in which these two variables are involved

The RH010 mutant was also complemented in trans with the high-affinity K⁺ transporter KtrAB from *Vibrio alginolyticus* [42] and analysed as described before (Fig. 2J–M). The degree of induction of *kdpFABC* in the complemented mutant was comparable to that in the wild type (Fig. 2J–M). However, the dynamics of transcription was qualitatively similar to that observed for the RH010 mutant, albeit over a more restricted dynamic range. The time-courses of the extra- and intracellular K⁺ concentrations showed the same qualitative behaviour as in the wild type. However, the intracellular concentrations of free and bound K⁺ were approximately 30% lower than those measured for the wild type. Hence, the mathematical model of the wild type was modified to match this situation. We added another uptake term

$$r_{Ktr} = V_{max,Ktr} \frac{K_{ext}^+}{K_{M,Ktr}^+ + K_{ext}^+}$$

to describe the uptake by KtrAB, and the parameters $V_{max,Ktr}$ and

$K_{M,Ktr}$ were adjusted in accordance with the measured K⁺ data. With these modifications, the model was found to reproduce the experimental findings quite well.

Supporting Information

Figure S1 Proteolysis controls appropriate KdpFABC level. *E. coli* MG1655 *rpsL150* (wild type) and *E. coli* RH010 were cultivated in phosphate buffered minimal medium containing 10 mM K⁺ up to the mid-logarithmic growth phase, exposed to extreme K⁺ limitation (0.04 mM K⁺) for 10 min to activate *kdpFABC* expression before proteins were labelled with ³⁵S-methionine. Labelling of *de novo* synthesized proteins was quenched by adding an excess of non-labelled methionine after 10 min. Protein turnover is determined by the reduction of the labelled protein complex over the time. At different times, samples were taken, immunoprecipitated with α KdpFABC antiserum, subjected to SDS-PAGE, and the amount of KdpFABC was quantified from the autoradiographies of the gels. The data represent one of three independently performed characteristic experiments. Half-life was determined to be 36.7 min for wild type KdpFABC and 28.4 min KdpFABC(G345S)BC. (TIF)

Table S1 Total and viable cell numbers and cytoplasmic volume after exposure of *E. coli* to K⁺ limitation. *E. coli* MG1655 cells were grown in minimal medium containing 10 mM K⁺ to the mid-logarithmic growth phase and shifted to K⁺ limitation (40 μ M K⁺). At the indicated times, cells were harvested, and the total and viable cell numbers as well as the cytoplasmic volume of the cells were determined as described in Materials and Methods. The values represent average values of at least three independent experiments. Standard deviations were below 5%. n.d., not determined. (DOCX)

Acknowledgements

We thank E.P. Bakker and I. Hänelt for providing plasmid pKT84.

Author Contributions

Conceived and designed the experiments: RH KJ JB AK. Performed the experiments: RH KZ SG MRF. Analyzed the data: RH SG AK KJ. Wrote the paper: RH SG AK KJ. Performed the biological experiments: RH KZ. Performed modeling experiments: SG MRF. Designed and coordinated the biological experiments: KJ RH. Designed and coordinated modeling experiments: AK JB.

References

- Epstein W (2003) The roles and regulation of potassium in bacteria. *Prog Nucleic Acid Res Mol Biol* 75: 293–320.
- Booth IR (1985) Regulation of cytoplasmic pH in bacteria. *Microbiol Rev* 49: 359–378.
- Sueller CH (1970) Enzymes activated by monovalent cations. *Science* 168: 789–795.
- Rübenhagen R, Morbach S, Krämer R (2001) The osmoreactive betaine carrier BetP from *Corynebacterium glutamicum* is a sensor for cytoplasmic K⁺. *EMBO J* 20: 5412–5420. doi:10.1093/emboj/20.19.5412.
- Giaever HM, Styrvold OB, Kaasen I, Strøm AR (1988) Biochemical and genetic characterization of osmoregulatory trehalose synthesis in *Escherichia coli*. *J Bacteriol* 170: 2841–2849.
- Sutherland L, Cairney J, Elmore MJ, Booth IR, Higgins CF (1986) Osmotic regulation of transcription: induction of the *proU* betaine transport gene is dependent on accumulation of intracellular potassium. *J Bacteriol* 168: 805–814.
- Lee SJ, Gralla JD (2004) Osmo-regulation of bacterial transcription via poised RNA polymerase. *Mol Cell* 14: 153–162.
- Nissen P, Hansen J, Ban N, Moore PB, Steitz TA (2000) The structural basis of ribosome activity in peptide bond synthesis. *Science* 289: 920–930.
- Csonka LN, Hanson AD (1991) Prokaryotic osmoregulation: genetics and physiology. *Annu Rev Microbiol* 45: 569–606. doi:10.1146/annurev.mi.45.100191.003033.
- Palleros DR, Reid KL, Shi L, Welch WJ, Fink AL (1993) ATP-induced protein-Hsp70 complex dissociation requires K⁺ but not ATP hydrolysis. *Nature* 365: 664–666. doi:10.1038/365664a0.
- Schlösser A, Meldorf M, Stumpe S, Bakker EP, Epstein W (1995) TrkH and its homolog, TrkG, determine the specificity and kinetics of cation transport by the Trk system of *Escherichia coli*. *J Bacteriol* 177: 1908–1910.
- Stumpe S, Bakker EP (1997) Requirement of a large K⁺-uptake capacity and of extracytoplasmic protease activity for protamine resistance of *Escherichia coli*. *Arch Microbiol* 167: 126–136.
- Ballal A, Basu B, Apte SK (2007) The Kdp-ATPase system and its regulation. *J Biosci* 32: 559–568.
- Altendorf K, Siebers A, Epstein W (1992) The Kdp-ATPase of *Escherichia coli*. *Ann N Y Acad Sci* 671: 228–243.
- Laimins LA, Rhoads DB, Epstein W (1981) Osmotic control of *kdp* operon expression in *Escherichia coli*. *Proc Natl Acad Sci USA* 78: 464–468.
- Walderhaug MO, Polarek JW, Voelkner P, Daniel JM, Hesse JE, et al. (1992) KdpD and KdpE, proteins that control expression of the *kdpABC* operon, are

- members of the two-component sensor-effector class of regulators. *J Bacteriol* 174: 2152–2159.
17. Heermann R, Jung K (2010) The complexity of the “simple” two-component system KdpD/KdpE in *Escherichia coli*. *FEMS Microbiol Lett* 304: 97–106. doi:10.1111/j.1574-6968.2010.01906.x.
 18. Heermann R, Jung K (2012) K⁺ supply, osmotic stress and the KdpD/KdpE two-component system. In: Gross R, Beier D, editors. Two-component systems in bacteria. Norwich, UK: Caister Academic Press. pp. 181–198.
 19. Voelkner P, Puppe W, Altendorf K (1993) Characterization of the KdpD protein, the sensor kinase of the K⁺-translocating Kdp system of *Escherichia coli*. *Eur J Biochem* 217: 1019–1026.
 20. Sugiura A, Nakashima K, Tanaka K, Mizuno T (1992) Clarification of the structural and functional features of the osmoregulated *kdp* operon of *Escherichia coli*. *Mol Microbiol* 6: 1769–1776.
 21. Jung K, Tjaden B, Altendorf K (1997) Purification, reconstitution, and characterization of KdpD, the turgor sensor of *Escherichia coli*. *J Biol Chem* 272: 10847–10852.
 22. Malli R, Epstein W (1998) Expression of the Kdp-ATPase is consistent with regulation by turgor pressure. *J Bacteriol* 180: 5102–5108.
 23. Hamann K, Zimmann P, Altendorf K (2008) Reduction of turgor is not the stimulus for the sensor kinase KdpD of *Escherichia coli*. *J Bacteriol* 190: 2360–2367. doi:10.1128/JB.01635-07.
 24. Asha H, Gowrishankar J (1993) Regulation of *kdp* operon expression in *Escherichia coli*: evidence against turgor as signal for transcriptional control. *J Bacteriol* 175: 4528–4537.
 25. Frymier JS, Reed TD, Fletcher SA, Csonka LN (1997) Characterization of transcriptional regulation of the *kdp* operon of *Salmonella typhimurium*. *J Bacteriol* 179: 3061–3063.
 26. Roe AJ, McLaggan D, O’Byrne CP, Booth IR (2000) Rapid inactivation of the *Escherichia coli* Kdp K⁺ uptake system by high potassium concentrations. *Mol Microbiol* 35: 1235–1243.
 27. Jung K, Krabusch M, Altendorf K (2001) Cs⁺ induces the *kdp* operon of *Escherichia coli* by lowering the intracellular K⁺ concentration. *J Bacteriol* 183: 3800–3803. doi:10.1128/JB.183.12.3800-3803.2001.
 28. Yan H, Fukamachi T, Saito H, Kobayashi H (2011) Expression and activity of Kdp under acidic conditions in *Escherichia coli*. *Biol Pharm Bull* 34: 426–429.
 29. Jung K, Veen M, Altendorf K (2000) K⁺ and ionic strength directly influence the autophosphorylation activity of the putative turgor sensor KdpD of *Escherichia coli*. *Journal of Biological Chemistry* 275: 40142–40147. doi:10.1074/jbc.M008917200.
 30. Heermann R, Weber A, Mayer B, Ott M, Hauser E, et al. (2009) The universal stress protein UspC scaffolds the KdpD/KdpE signaling cascade of *Escherichia coli* under salt stress. *J Mol Biol* 386: 134–148. doi:10.1016/j.jmb.2008.12.007.
 31. Lüttmann D, Heermann R, Zimmer B, Hillmann A, Rampp IS, et al. (2009) Stimulation of the potassium sensor KdpD kinase activity by interaction with the phosphotransferase protein IIA^{Ntr} in *Escherichia coli*. *Mol Microbiol* 72: 978–994. doi:10.1111/j.1365-2958.2009.06704.x.
 32. Laermann V, Čudić E, Kipschull K, Zimmann P, Altendorf K (2013) The sensor kinase KdpD of *Escherichia coli* senses external K⁺. *Mol Microbiol* 88: 1194–1204. doi:10.1111/mmi.12251.
 33. Jung K, Altendorf K (1998) Individual substitutions of clustered arginine residues of the sensor kinase KdpD of *Escherichia coli* modulate the ratio of kinase to phosphatase activity. *J Biol Chem* 273: 26415–26420.
 34. Heermann R, Altendorf K, Jung K (2000) The hydrophilic N-terminal domain complements the membrane-anchored C-terminal domain of the sensor kinase KdpD of *Escherichia coli*. *J Biol Chem* 275: 17080–17085. doi:10.1074/jbc.M000093200.
 35. Heermann R, Lippert M-L, Jung K (2009) Domain swapping reveals that the N-terminal domain of the sensor kinase KdpD in *Escherichia coli* is important for signaling. *BMC Microbiol* 9: 133. doi:10.1186/1471-2180-9-133.
 36. Kremling A, Heermann R, Centler F, Jung K, Gilles ED (2004) Analysis of two-component signal transduction by mathematical modeling using the KdpD/KdpE system of *Escherichia coli*. *Biosystems* 78: 23–37. doi:10.1016/j.biosystems.2004.06.003.
 37. Trchounian A, Kobayashi H (1999) Kup is the major K⁺ uptake system in *Escherichia coli* upon hyper-osmotic stress at a low pH. *FEBS Letters* 447: 144–148.
 38. McLaggan D, Naprstek J, Buurman ET, Epstein W (1994) Interdependence of K⁺ and glutamate accumulation during osmotic adaptation of *Escherichia coli*. *J Biol Chem* 269: 1911–1917.
 39. Epstein W, Davies M (1970) Potassium-dependant mutants of *Escherichia coli* K-12. *J Bacteriol* 101: 836–843.
 40. Heermann R, Zeppenfeld T, Jung K (2008) Simple generation of site-directed point mutations in the *Escherichia coli* chromosome using Red[®]/ET[®] Recombination. *Microb Cell Fact* 7: 14. doi:10.1186/1475-2859-7-14.
 41. Bertrand J, Altendorf K, Bramkamp M (2004) Amino acid substitutions in putative selectivity filter regions III and IV in KdpA alter ion selectivity of the KdpFABC complex from *Escherichia coli*. *J Bacteriol* 186: 5519–5522. doi:10.1128/JB.186.16.5519-5522.2004.
 42. Nakamura T, Yuda R, Unemoto T, Bakker EP (1998) KtrAB, a new type of bacterial K⁺-uptake system from *Vibrio alginolyticus*. *J Bacteriol* 180: 3491–3494.
 43. Rodríguez-Fernández M, Banga JR (2010) SensSB: a software toolbox for the development and sensitivity analysis of systems biology models. *Bioinformatics* 26: 1675–1676. doi:10.1093/bioinformatics/btq242.
 44. Fritz G, Koller C, Burdack K, Tetsch L, Haneburger I, et al. (2009) Induction kinetics of a conditional pH stress response system in *Escherichia coli*. *J Mol Biol* 393: 272–286. doi:10.1016/j.jmb.2009.08.037.
 45. Blattner FR, Plunkett G, Bloch CA, Perna NT, Burland V, et al. (1997) The complete genome sequence of *Escherichia coli* K-12. *Science* 277: 1453–1462.
 46. Epstein W, Kim BS (1971) Potassium transport loci in *Escherichia coli* K-12. *J Bacteriol* 108: 639–644.
 47. Aiba H, Adhya S, de Crombrugge B (1981) Evidence for two functional *gal* promoters in intact *Escherichia coli* cells. *J Biol Chem* 256: 11905–11910.
 48. Livak KJ, Schmittgen TD (2001) Analysis of relative gene expression data using real-time quantitative PCR and the 2^{-ΔΔC_T} Method. *Methods* 25: 402–408. doi:10.1006/meth.2001.1262.
 49. Bossemeyer D, Borchard A, Dosch DC, Helmer GC, Epstein W, et al. (1989) K⁺-transport protein TrkA of *Escherichia coli* is a peripheral membrane protein that requires other *trk* gene products for attachment to the cytoplasmic membrane. *J Biol Chem* 264: 16403–16410.
 50. Stock JB, Rauch B, Roseman S (1977) Periplasmic space in *Salmonella typhimurium* and *Escherichia coli*. *J Biol Chem* 252: 7850–7861.
 51. Cayley S, Lewis BA, Guttman HJ, Record MT (1991) Characterization of the cytoplasm of *Escherichia coli* K-12 as a function of external osmolarity. Implications for protein-DNA interactions in vivo. *J Mol Biol* 222: 281–300.
 52. Fulton AB (1982) How crowded is the cytoplasm? *Cell* 30: 345–347.
 53. Laemmli UK (1970) Cleavage of structural proteins during the assembly of the head of bacteriophage T4. *Nature* 227: 680–685. doi:10.1038/227680a0.
 54. Lee SB, Bailey JE (1984) Genetically structured models for lac promoter-operator function in the *Escherichia coli* chromosome and in multicopy plasmids: Lac operator function. *Biotechnol Bioeng* 26: 1372–1382. doi:10.1002/bit.260261115.
 55. Nelder JA (1961) The fitting of a generalization of the logistic curve. *Biometrics* 17: 89–110.
 56. Rhoads DB, Epstein W (1978) Cation transport in *Escherichia coli*. IX. Regulation of K⁺ transport. *J Gen Physiol* 72: 283–295.